
Research Article: New Research | Sensory and Motor Systems

A somatosensory computation that unifies limbs and tools

<https://doi.org/10.1523/ENEURO.0095-23.2023>

Cite as: eNeuro 2023; 10.1523/ENEURO.0095-23.2023

Received: 22 March 2023

Revised: 13 September 2023

Accepted: 25 September 2023

This Early Release article has been peer-reviewed and accepted, but has not been through the composition and copyediting processes. The final version may differ slightly in style or formatting and will contain links to any extended data.

Alerts: Sign up at www.eneuro.org/alerts to receive customized email alerts when the fully formatted version of this article is published.

Copyright © 2023 Miller et al.

This is an open-access article distributed under the terms of the Creative Commons Attribution 4.0 International license, which permits unrestricted use, distribution and reproduction in any medium provided that the original work is properly attributed.

1 **Manuscript Title:** A somatosensory computation that unifies limbs and tools

2 **Abbreviated Title:** Computationally unifying limbs and tools

3 **Authors:**

4 Luke E. Miller¹⁻⁴, Cécile Fabio¹⁻³, Frédérique de Vignemont⁷, Alice Roy⁶, W. Pieter
5 Medendorp^{4,8} & Alessandro Farnè^{1-3,5,8}

1. Integrative Multisensory Perception Action & Cognition Team - ImpAct, Lyon Neuroscience
Research Center, INSERM U1028, CNRS U5292; Bron, France

2. University of Lyon 1; Villeurbanne, France

3. Hospices Civils de Lyon, Neuro-immersion ; Bron, France

4. Radboud University, Donders Institute for Brain, Cognition and Behaviour; Nijmegen, The
Netherlands

5. Center for Mind/Brain Sciences, University of Trento; Rovereto, Italy

6. Laboratoire Dynamique Du Langage, CNRS UMR 5596, Lyon, France

7. Institut Jean Nicod, Department of cognitive studies, Ecole Normale Supérieure, PSL University,
Paris, France

8. These authors contributed equally to the study

Correspondence should be addressed to: Luke E. Miller, Luke.Miller@donders.ru.nl

6 **Number of figures:** 8

7 **Number of tables:** 1

8 **Number of multimedia:** 1

9 **Number of words for abstract:** 252

10 **Number of words for significance statement:** 120

11 **Number of words in Introduction:** 763

12 **Number of words in Discussion:** 1450

13 **Author Contributions**

14 L.E.M., C.F., and A.F. conceived of the behavioral experiments; C.F. performed the
15 behavioral experiments; L.E.M. and C.F. analyzed the behavioral data; L.E.M., A.F., and
16 W.P.M. conceived of the computational model; L.E.M and W.P.M. conceived the neural
17 network model; F.V. and A.R. provided conceptual input; L.E.M., A.F. and W.P.M. wrote the
18 original draft of the manuscript; All authors provided feedback on the manuscript and
19 approved its final form.

20 **Competing interests**

21 The authors declare no competing interests.

1 **A somatosensory computation that unifies limbs and tools**

2 **Abstract**

3 It is often claimed that tools are embodied by their user, but whether the brain actually re-
4 purposes its body-based computations to perform similar tasks with tools is not known. A
5 fundamental computation for localizing touch on the body is *trilateration*. Here, the location
6 of touch on a limb is computed by integrating estimates of the distance between sensory in-
7 put and its boundaries (e.g., elbow and wrist of the forearm). As evidence of this computa-
8 tional mechanism, tactile localization on a limb is most precise near its boundaries and low-
9 est in the middle. Here we show that the brain repurposes trilateration to localize touch on a
10 tool, despite large differences in initial sensory input compared to touch on the body. In a
11 large sample of participants, we found that localizing touch on a tool produced the signature
12 of trilateration, with highest precision close to the base and tip of the tool. A computational
13 model of trilateration provided a good fit to the observed localization behavior. To further
14 demonstrate the computational plausibility of repurposing trilateration, we implemented it in
15 a three-layer neural network that was based on principles of probabilistic population coding.
16 This network determined hit location in tool-centered coordinates by using a tool's unique
17 pattern of vibrations when contacting an object. Simulations demonstrated the expected sig-
18 nature of trilateration, in line with the behavioral patterns. Our results have important implica-
19 tions for how trilateration may be implemented by somatosensory neural populations. We
20 conclude that trilateration is likely a fundamental spatial computation that unifies limbs and
21 tools.

22 **Significance statement**

23 It is often claimed that tools are embodied by the user, but computational evidence for this
24 claim is scarce. We show that to localize touch on a tool, the brain repurposes a fundamen-
25 tal computation for localizing touch on the body, *trilateration*. A signature of trilateration is
26 high localization precision near the boundaries of a limb and low precision in the middle. We
27 find that localizing touch on a tool produces this signature of trilateration, which we charac-
28 terize using a computational model. We further demonstrate the plausibility of embodiment
29 by implementing trilateration within a three-layer neural network that transforms a tool's vi-
30 brations into a tool-centered spatial representation. We conclude that trilateration is a fun-
31 damental spatial computation that unifies limbs and tools.

32 Introduction

33 The proposal that the brain treats a tool as if it were an extended limb (tool embodiment)
34 was first made over a century ago (Head and Holmes, 1911). From the point of view of
35 modern neuroscience, embodiment would entail that the brain reuses its sensorimotor com-
36 putations when performing the same task with a tool as with a limb. There is *indirect* evi-
37 dence that this is the case (for reviews, see Maravita and Iriki, 2004; Martel et al., 2016),
38 such as the ability of tool-users to accurately localize where a tool has been touched (Miller
39 et al., 2018) just as they would on their own body. Several studies have highlighted im-
40 portant similarities between tool-based and body-based tactile spatial processing
41 (Yamamoto and Kitazawa, 2001; Kilteni and Ehrsson, 2017; Miller et al., 2018), including at
42 the neural level in the activity of fronto-parietal regions (Miller et al., 2019; Pazen et al.,
43 2020; Fabio et al., 2021). Tool use also modulates somatosensory perception and action
44 processes (Cardinali et al., 2009; Cardinali et al., 2011; Cardinali et al., 2012; Sposito et al.,
45 2012; Canzoneri et al., 2013; Miller et al., 2014; Garbarini et al., 2015; Cardinali et al., 2016;
46 Miller et al., 2017; Martel et al., 2019; Romano et al., 2019; Miller et al., 2019b).

47 The above findings are suggestive that functional similarities between tools and limbs
48 exist. However, *direct* evidence that body-based computational mechanisms are repurposed
49 to sense and act with tools is lacking. For this to be possible, the nervous system would
50 need to resolve the differences in the sensory input following touch on the skin or a tool. Un-
51 like the skin, tools are not innervated with mechanoreceptors. Touch location is instead ini-
52 tially encoded in the tool's mechanical response; for example, in how it vibrates when strik-
53 ing an object (Miller et al., 2018). Repurposing a body-based neural computation to perform
54 the same function for a tool (i.e., embodiment) requires overcoming this key difference in the
55 sensory input signal. The present study uses tool-based tactile localization (Miller et al.,
56 2018) as a case study to provide the first neurocomputational test of embodiment.

57 Tactile localization on the body is often characterized by greater precision near body-
58 part boundaries (e.g., joints or borders), a phenomenon called perceptual anchoring

59 (Cholewiak and Collins, 2003; de Vignemont et al., 2009). A recent study found converging
60 evidence that perceptual anchors are the signature of *trilateration* (Miller et al., 2022), a
61 computation used by surveyors to localize an object within a map. To do so, a surveyor es-
62 timates the object's distance from multiple landmarks of known positions. When applied to
63 body maps (Figure 1A, bottom), a 'neural surveyor' localizes touch on a body part by esti-
64 mating the distance between sensory input and body-part boundaries (e.g., the wrist and
65 elbow for the forearm). To estimate the touch location in limb-centered coordinates, these
66 two distance estimates can be integrated to produce a Bayes-optimal location percept (Ernst
67 and Banks, 2002; Kording and Wolpert, 2004; Clemens et al., 2011). Consistent with We-
68 ber's Law and log-coded spatial representations (Petzschner et al., 2015), noise in each dis-
69 tance estimate increased linearly as a function of distance (Figure 1B). Integrating them re-
70 sulted in an inverted U-shaped noise profile across the surface, with the lowest noise near
71 the boundaries and highest noise in the middle (i.e., perceptual anchoring).

72 In the present study, we investigated whether trilateration is repurposed to localize
73 touch a tool (Figure 1A). If this is indeed the case, localizing touch on a tool would be char-
74 acterized by an inverted U-shaped pattern of variable errors across its surface (Figure 1B).
75 We first provide a theoretical formulation of how trilateration could be repurposed to sense
76 with a tool, arguing that the brain uses the tool's vibrational properties to stand-in for a rep-
77 resentation for the physical space of the tool (Miller et al., 2018). In this formulation, trilatera-
78 tion is repurposed by computing over a vibratory feature space (Figure 2), using its bounda-
79 ries as proxies for the boundaries of physical tool space. Distance estimates (Figure 1A) are
80 then computed within a neural representation of the feature space, just like they would be for
81 a representation of body space. Next, we characterize the ability of participants to localize
82 touch on a tool (Figure 1C) and use computational modelling to verify the expected compu-
83 tational signature of trilateration (Figure 1B). Finally, we use neural network modelling to im-
84 plement the vibration-to-location transformation required for trilaterating touch location on a
85 tool, providing one possible mechanism for how embodiment is implemented. In all, our find-

86 ings solidify the plausibility of trilateration as the computation underlying tactile localization
87 on both limbs and tools.

88 **Material and Methods**

89 **Theoretical formulation of trilateration**

90 In the present section, we provide a theoretical formulation of trilateration and how it can be
91 applied to localizing touch within a somatosensory-derived coordinate system, be it centered
92 on a body part or the surface of a tool (Figure 1A). The general *computational goal* of trilat-
93 eration is to estimate the location of an object by calculating its distance from vantage points
94 of known position, which we will refer to as landmarks. Applied to tactile localization, this
95 amounts to estimating the location of touch by averaging over distance estimates taken from
96 the boundaries of the sensory surface (Figure 1A), which serve as the landmarks and are
97 assumed to be known to the nervous system via either learning or sensory feedback (Longo
98 et al., 2010). For a body part (e.g., forearm), the landmarks are often its joints (e.g., wrist
99 and elbow) and lateral sides. For simple tools such as rods, the landmarks correspond to
100 their handle and tip—previous research has shown that users can sense their positions from
101 somatosensory feedback during welding (Debats et al., 2012).

102 We will first consider the general case of localizing touch within an unspecified soma-
103 tosensory coordinate system. For simplicity, we will consider only a single dimension of the
104 coordinate system, with localization between its two boundaries. We propose that the soma-
105 tosensory system only needs three spatial variables, $\{x_1, x_2, x_3\}$, to derive an estimate \tilde{L} of
106 the actual location of touch L in surface-centered coordinates. The variables x_1 and x_2 cor-
107 respond to the proximal and distal boundaries, respectively. The variable x_3 corresponds to
108 the sensory input. Due to noise (Faisal et al., 2008), the nervous system does not represent
109 variables as point estimates but as probability densities over some range of values (Pouget

110 et al., 2013). Assuming normally-distributed noise, each variable x_i can be thus thought of
 111 as a Gaussian likelihood

$$p(x_i|X_i) = N(X_i, \sigma_i^2) \quad (1)$$

112 where the mean X_i corresponds to its true spatial position and the variance σ_i^2 corresponds
 113 to the uncertainty in its internal estimate. Here, X_1 and X_2 are the true positions of the land-
 114 marks (i.e., boundaries) and X_3 is the position of the sensory input. It is important to note
 115 here that these positions can be specified within any shared coordinate system. For exam-
 116 ple, touch on the body is thought to initially be represented in skin-based coordinates
 117 (Medina and Coslett, 2010), not coordinates centered on a limb. The relationship between
 118 X_3 and L therefore remains ambiguous without the proper computation to transform it into
 119 the actual surface-centered coordinates (Longo et al., 2010).

120 Trilateration performs the necessary computation to transform x_3 into surface-
 121 centered coordinates (Miller et al., 2022). It does so by calculating its distance from the prox-
 122 imal and distal boundaries of the coordinate system (x_1 and x_2 , respectively), producing two
 123 additional estimates:

$$\begin{aligned} p(d_1|x_1, x_3) &= N(X_3 - X_1, \sigma_1^2(d_1)) \\ p(d_2|x_2, x_3) &= N(X_2 - X_3, \sigma_2^2(d_2)) \end{aligned} \quad (2)$$

124 where each distance estimate d_i corresponds to a Gaussian likelihood with a mean equal to
 125 the distance between X_3 and the respective boundary and a variance that scales with dis-
 126 tance. That is, localization estimates are more precise when the touch is physically closer to
 127 a boundary than when it is farther away (Figure 1B). This distance-dependent noise is con-
 128 sistent with coding distance in log space (Petzschner et al., 2015) and is a consequence of
 129 how distance computation is implemented by a neural decoder (see below).

130 Given the above distance estimates (Eq. 2), we can derive two estimates of touch lo-
 131 cation \tilde{L}_i that are aligned within a common coordinate system:

$$p(\tilde{L}_1|L) = p(x_1|X_1) + p(d_1|x_1, x_3) \quad (3)$$

$$p(\tilde{L}_2|L) = p(x_2|X_2) - p(d_2|x_2, x_3)$$

132 These two location estimates can be used to derive a final estimate. However, given the
 133 presence of distance-dependent noise, the precision of each estimate will vary across the
 134 sensory surface (Figure 1B). Assuming a flat prior for touch location, the statistically optimal
 135 solution (i.e., maximum likelihood) is to integrate both estimates:

$$p(L|\tilde{L}_1, \tilde{L}_2) \propto p(\tilde{L}_1|L)p(\tilde{L}_2|L) \quad (4)$$

136 Here, the mean (μ_{INT}) and variance (σ_{INT}^2) of the integrated surface-centered posterior dis-
 137 tribution depend on the means (μ_1 and μ_2) variances (σ_1^2 and σ_2^2) of the individual estimates:

$$\mu_{INT} = \left(\frac{\mu_1}{\sigma_1^2} + \frac{\mu_2}{\sigma_2^2} \right) \sigma_{INT}^2 \quad , \quad \sigma_{INT}^2 = \frac{\sigma_1^2 \sigma_2^2}{\sigma_1^2 + \sigma_2^2} \quad (5)$$

138 The integrated posterior $p(L|\tilde{L}_1, \tilde{L}_2)$ thus reflects the maximum-likelihood estimate of touch
 139 location L . Given that the noise in each individual estimate scales linearly with distance, in-
 140 tegration has the consequence of producing an inverted U-shaped pattern of variance (Fig-
 141 ure 1B). This pattern of variability serves as a *computational signature* of trilateration, which
 142 has been observed for tactile localization on the arm and fingers (Miller et al., 2022). The
 143 present study investigates whether this is the case for localizing touch on a hand-held rod.
 144 Our computational analyses implement this probabilistic model of trilateration (see below).

145 **Computing a tool-centered spatial code with trilateration**

146 Let us now consider the more specific case of performing trilateration for touch on a tool
 147 (Figure 1A, top). Because the tool surface is not innervated, spatial information does not
 148 arise from a distribution of receptors but must instead be inferred from sensory information

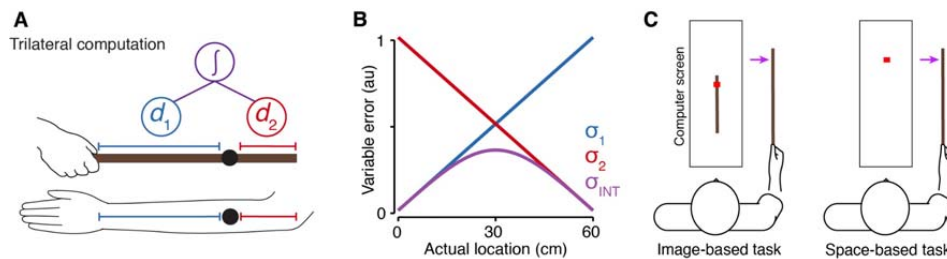


Figure 1. Model of trilateration and tool-sensing paradigm

(A) The trilateral computation applied to the space of the arm (bottom) a hand-held rod (top). Distance estimates from sensory input (black) and each boundary (d_1 and d_2) are integrated (purple) to form a location estimate. (B) In our model, the noise in each distance estimate (d_1 , d_2) increases linearly with distance. The integrated estimate forms an inverted U-shaped pattern. (C) Two tool-sensing tasks used to characterize tactile localization on a hand-held rod. The purple arrow corresponds to the location of touch in tool-centered space. The red square corresponds to the judgment of location within the computer screen.

149 during tool-object contact. However, as we will see, this information forms a feature space
 150 that can computationally stand in for the real physical space of the tool (Figure 2). Trilatera-
 151 tion can be performed on this feature space, leading to a tool-centered code.

152 As with the body, the somatosensory system needs three variables, $\{x_1, x_2, x_3\}$, to
 153 derive an estimate \tilde{L} of the actual location of touch L in tool-centered coordinates. The rep-
 154 resentational nature of these variables depends on the type of sensory information that en-
 155 codes where a tool was touched. We have previously argued that touch location is encoded
 156 in rod's resonant frequencies (Miller et al., 2018). The frequencies of these modes are de-
 157 termined by the physical properties of the rod, such as its length and material. However, the
 158 relative amplitude of each mode is determined by touch location (Figure 2A), a pattern that is

159 invariant across rods. The link between location and amplitude is captured by the shape of
 160 the modes.

161 Touch location can therefore be encoded in a unique combination of modal ampli-
 162 tudes, called *vibratory motifs*. These motifs form a multidimensional feature space that forms
 163 a vibration-to-location isomorphism (Figure 2B). Theoretically, this isomorphic mapping be-
 164 tween the feature space of the vibrations and tool-centered space can computationally stand
 165 in for the physical space of the rod. We can therefore re-conceptualize the three initial spa-
 166 tial variables, $\{x_1, x_2, x_3\}$, in relation to the isomorphism. The estimates x_1 and x_2 encode the
 167 location of the proximal and distal boundaries within the feature space, respectively. The es-
 168 timate x_3 encodes the sensory input, which in our case is the vibration amplitude in each
 169 mode. Once the nervous system has learned the isomorphic mapping, the trilateral compu-
 170 tation (Equations 2-5) can be used to derive an estimate of the tool-centered location of
 171 touch (Figure 2B). To concretely demonstrate this possibility, we implemented this isomor-
 172 phic mapping in a simple neural network.

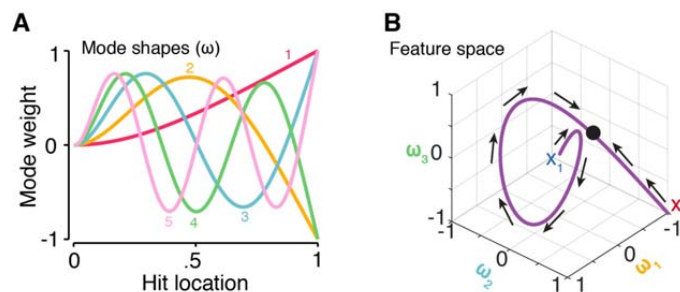


Figure 2. Vibration modes and feature space

(A) The shape of the first five modes ω for contact on a cantilever rod. The weight of each mode varies as a function of hit location. Each hit location is characterized by a unique combination of mode weights. (B) The vibration-location feature space (purple) from handle (X_1) to tip (X_2). This feature space is isomorphic with the actual physical space of the rod. ω corresponds to a resonant frequency, the black dot corresponds to the hit location (as in Figure 1A) within the feature space, and the arrows are the gradients of distance estimation during trilateration.

173 **Neural network implementation for trilateration on a tool**

174 Somatosensory regions are characterized by spatial maps of the surface of individual body
175 parts (Penfield and Boldrey, 1937). Based on this notion, the above formulation of trilatera-
176 tion to tactile localization on the body surface was implemented in a biologically inspired two-
177 layer feedforward neural network (Miller et al., 2022). The first layer consisted of units that
178 were broadly tuned to touch location in skin-based coordinates, as is thought to be encoded
179 by primary somatosensory cortex. The second layer consisted of units whose tuning was
180 characterized by distance-dependent gradients (either in peak firing rate and/or tuning width)
181 that were anchored to one of the joints. They therefore embodied the distance computation
182 as specified in Equations 2–3. A Bayesian decoder demonstrated that the behavior of this
183 network matched what would be expected by optimal trilateration (Equations 2–5), display-
184 ing distance-dependent noise and an inverted U-shaped variability following integration.

185 While this network relies on the observation that individual primary somatosensory
186 neurons are typically tuned to individual regions of the skin (Delhayé et al., 2018), can it also
187 be re-used for performing trilateration in vibration space? The vibratory motifs are unlikely to
188 be spatially organized across the cortical surface. Instead, the nervous system must internal-
189 ize the isomorphic mapping between the motifs and the physical space of the tool (Figure 2).
190 Disrupting the expected vibrations disrupts localization (Miller et al., 2018), suggesting that
191 the user has internal models of rod dynamics (Imamizu et al., 2000). We assume that this
192 internal model is implemented in units that are tuned to the statistics of the vibratory motifs.

193 We implemented the trilateral computation (Equations 2–5) in a three-layer neural
194 network with four processing stages (Figure 3): First, the amplitudes of each mode are esti-
195 mated by a population of units with subpopulations tuned to each resonant mode (Layer 1).
196 Second, activation in each subpopulation is integrated by units tuned to the multidimensional
197 statistics of the motifs (Layer 2). This layer effectively forms the internal model of the feature
198 space that is isomorphic to the rod's physical space. Next, this activation pattern is trans-
199 formed into tool-centered coordinates (Equations 2–3) via two decoding subpopulations
200 whose units are tuned to distance from the boundaries of the feature space (Eq. 3; Layer 3).

201 The population activity of each decoding subpopulations reflects the likelihoods in Equa-
 202 tion 4 (Jazayeri and Movshon, 2006). Lastly, the final tool-centered location estimate is de-
 203 rived by a Bayesian decoder (Ma et al., 2006) that integrates the activity of both subpopula-
 204 tions (Eq. 5).

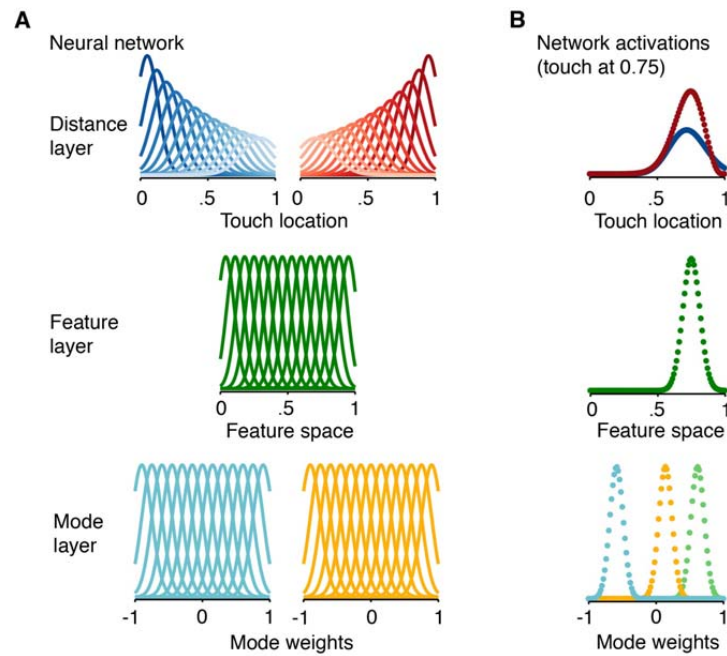


Figure 3. Neural network implementation of trilateration

(A) Neural network implementation of trilateration: (lower panel) the Mode layer is composed of subpopulations (two shown here) sensitive to the weight of individual modes (see Figure 2A), which are location-dependent; (middle panel) the Feature layer takes input from the mode layer and encodes the feature space (see Figure 2B), which forms the isomorphism with the physical space of the tool; (upper panel) the Distance layer is composed of two subpopulations of neurons with distance-dependent gradients in tuning properties (shown: firing rate and tuning width). The distance of a tuning curve from its “anchor” is coded by the luminance, with darker colors corresponding to neurons that are closer to the spatial boundary.

(B) Activations for each layer of the network averaged over 5000 simulations when touch was at 0.75 (space between 0 and 1). Each dot corresponds to a unit of the neural network. (lower panel) mode layer, with three of five subpopulations shown; (middle panel) feature layer; (upper panel) distance layer of localization for each decoding subpopulation.

205 The feature space of vibrations is multidimensional, composed of a theoretically infi-
 206 nite number of modes. However, only the first five modes (Figure 2A) are typically within the
 207 bandwidth of mechanoreceptors (i.e., ~10-1000 Hz; Johansson and Flanagan, 2009). The
 208 first layer of our network was therefore composed of units tuned to the amplitudes of these
 209 modes (Figure 3A, bottom). This layer was composed of five subpopulations that each en-
 210 code an estimate of the amplitude of a specific mode. These units were broadly-tuned with
 211 Gaussian (bell-shaped) tuning curves f^M of the following form:

$$f^M(\theta) = \kappa \left(\exp \left[\frac{-(\theta - \mu)^2}{2\sigma^2} \right] \right) \quad (6)$$

212 where κ is the peak firing rate (i.e., gain), μ is the tuning center related to the amplitude of
 213 the specific mode, θ is the mode amplitude of the stimulus, and σ^2 is the variance of the tun-
 214 ing curve. We modelled the response properties of these units for a given contact location
 215 on the rod with likelihood functions $p(r_i^M|\theta)$ denoting the probability that mode amplitude θ
 216 caused r_i^E spikes in encoding unit i . The likelihood function $p(r_i^M|\theta)$ was modeled as a
 217 Poisson probability distribution with a Fano factor of one according to the following equation:

$$p(r_i^M|\theta) = \frac{e^{-f_i^M(\theta)} f_i^M(\theta)^{r_i^M}}{r_i^M!} \quad (7)$$

218 where f_i^M is the tuning curve of unit i . The population response of the encoding units is de-
 219 noted by a vector $\mathbf{r}^M \equiv \{r_1^M, \dots, r_N^M\}$, where r_i^M is the spike count of unit i .

220 The amplitude θ of each mode is tied directly to the stimulus location L (Miller et al.,
 221 2018). The function of the next layer is to integrate the estimated amplitudes of each mode,
 222 encoded in \mathbf{r}^M , into a representation of the feature space that can be directly linked to L . It

223 does so via units with bell-shaped tuning curves f^S over the feature space (Figure 3A, mid-
 224 dle). The population activity r^S of this layer is a combination of (1) the synaptic input $W^S \cdot r^M$,
 225 where ‘ \cdot ’ is the dot product and W^S is the matrix of all synaptic weights; and (2) the uninher-
 226 ited Poisson noise in the unit’s spiking behavior (Eq. 7). Each unit i in the second layer was
 227 fully connected to each unit in the first layer via a vector of synaptic weights w_i^S , which was
 228 set to be proportional to r^M for each touch location L . For simplicity, the input into the sec-
 229 ond layer ($f^S(j)$) corresponded to the winner-take-all of the synaptic input ($j = \operatorname{argmax}_L (W^S \cdot$
 230 $r^M)$).

231 The function of the third layer was to estimate the location of L in tool-centered coord-
 232 inates given the population response r^S in the feature space layer. We implemented this
 233 computation in two independent decoding subpopulations, each of which was “anchored” to
 234 one of the boundaries of the feature space (Figure 3A, top). The population activity r^D of
 235 each subpopulation corresponded to: $r_i^D = w_i^D \cdot r^S + \epsilon_i$, where w_i^D is the vector of synaptic
 236 weights connecting unit i to the second layer and ϵ_i is the uninherited Poisson noise in the
 237 unit’s spiking behavior (Eq. 7). Each unit in the decoding layer was fully connected to each
 238 unit in the encoding layer via w^D . We used the Matlab function *fmincon* to find the positive-
 239 valued weight vector that produced the decoding unit’s pre-specified tuning curve (see be-
 240 low).

241 As in the previous neural network for body-centered tactile localization (Miller et al.,
 242 2022), the distance computation (Equations 2–3) was embodied by distance-dependent gra-
 243 dients in the tuning of units f^D in each decoding subpopulation. The gain κ of these units
 244 formed a distance-dependent gradient (close-to-far: high-to-low gain) across the length of
 245 the feature space.

$$\kappa(d) = \frac{\kappa_0}{(1 + \beta d)^2} \quad (8)$$

246 where κ_0 corresponds to the gain of the tuning curve centered on the landmark’s location
 247 (i.e., distance zero), d is the distance from the center of the tuning curve ($d \geq 0$) and the

248 landmark, and β is a scaling factor. The width σ of each tuning curve can be uniform in ei-
 249 ther linear or log space. In the latter case, tuning width also forms a distance-dependent
 250 gradient (close-to-far: narrow-to-wide tuning) in linear space (Nieder and Miller, 2003), con-
 251 sistent with the Weber-Fechner law.

$$\sigma(d) = (\gamma \log(d + 1) + 1) \sigma_0 \quad (9)$$

252 where σ_0 corresponds to the width of the tuning curve centered on the landmark's location, d
 253 is the distance from the center of the tuning curve and the landmark ($d \geq 0$), and γ is a scal-
 254 ing factor. It is important to note that these units f^D are tuned to the feature space, not the
 255 vibrations themselves (as in the encoding layer). Given the isomorphism, we can therefore
 256 link their response properties directly to the location of touch L .

257 When neuronal noise is Poisson-like (as in Eq. 7), the gain of a neural population re-
 258 sponse reflects the precision (i.e., inverse variance) of its estimate (Ma et al., 2006). There-
 259 fore, given the aforementioned distance-dependent gradient in gain, noise in each subpopu-
 260 lation's location estimate (that is, its uncertainty) will increase as a function of distance from
 261 a landmark (i.e., the handle or tip). Consistent with several studies (Jazayeri and Movshon,
 262 2006; Ma et al., 2006), we assume that the population responses encode log probabilities.
 263 We can therefore decode a maximum likelihood estimates of each subpopulation as follows:

$$\begin{aligned} p(\tilde{L}_1 | L, \mathbf{r}^{D1}) &= \exp(\mathbf{h}^{D1}(L) \cdot \mathbf{r}^{D1}) \\ p(\tilde{L}_2 | L, \mathbf{r}^{D2}) &= \exp(\mathbf{h}^{D2}(L) \cdot \mathbf{r}^{D2}) \end{aligned} \quad (10)$$

264 where \mathbf{h}^D is a kernel and \mathbf{r}^D is the subpopulation response. When neural responses are
 265 characterized by independent Poisson noise (Eq. 7), \mathbf{h}^D is equivalent to the log of each sub-
 266 population's tuning curve f^D at value L (Jazayeri and Movshon, 2006; Ma et al., 2006). As-
 267 suming that the population response reflects log probabilities, optimally integrating both es-
 268 timates (Eq. 5) amounts to simply summing the activity of each subpopulation.

$$p(\tilde{L}_{INT}|L, \mathbf{r}^{D1}, \mathbf{r}^{D2}) = \exp(\mathbf{h}^{D1}(L) \cdot \mathbf{r}^{D1} + \mathbf{h}^{D2}(L) \cdot \mathbf{r}^{D2}) \quad (11)$$

269 where the optimal estimate \tilde{L}_{INT} on a given trial n can be written as the location for which the
 270 log-likelihood of the summed population responses is maximal.

$$\tilde{L}_{INT}^{(n)} = \operatorname{argmax}_L(\mathbf{h}^{D1}(L) \cdot \mathbf{r}^{D1} + \mathbf{h}^{D2}(L) \cdot \mathbf{r}^{D2}) \quad (12)$$

271 The above neural network, with a different encoding layer, implements trilateration
 272 for localizing touch in body-centered coordinates. Our present neural network (Equations 6–
 273 12) generalizes the Bayesian formulation of trilateration (Equations 2–5) to localizing touch
 274 on a tool, using a vibratory feature space as a proxy for tool-centered space. The flow of ac-
 275 tivity in this network can be visualized at Figure 3B, where the touch occurs at 75% the sur-
 276 face of the tool.

277 **Table 1. Neural network parameter values**

	f^M	f^S	f^{D1}	f^{D2}
μ	-1.5:02:1.5	-40:1:140	0:1:140	-40:1:100
κ or κ_0	25	25	25	25
σ or σ_0	0.08	3.40	3.40	3.40
β	—	—	0.01	0.01
γ	—	—	0.5	0.5

278 To systematically investigate the behavior of this network, we simulated 5000 in-
 279 stances of touch at a wide range of locations (10% to 90% of the space) on the tool surface
 280 using the above network. The input into the neural network were the mode amplitudes θ for
 281 the corresponding location L . For simplicity we did not model the actual process of mode de-
 282 composition from the spiking behavior of mechanoreceptors (Miller et al., 2018), but we did
 283 assume that the process is affected by sensory noise (Faisal et al., 2008). Therefore, for
 284 each simulation, the input ($\theta[L]$) was corrupted by Gaussian noise with a standard deviation

285 of 0.5 (units: % of space). The values for the above parameters in all layers can be seen in
286 Table 1. All units of each layer shared the same parameter values. We used a maximum
287 log-likelihood decoder to localize touch from the overall response of each subpopulation
288 separately or integrated.

289 **Behavioral Experiment**

290 *Participants*

291 Forty right-handed participants (24 females, 23.7 ± 2.5 years of age) in total completed our
292 behavioral experiments. Two participants were removed due to inability to follow task in-
293 structions, leaving thirty-eight in total to be analyzed. All participants had normal or correct-
294 ed-to-normal vision and no history of neurological impairment. Every participant gave in-
295 formed consent before the experiment. The study was approved by the ethics committee
296 (CPP SUD EST IV, Lyon, France).

297 *Experimental procedure*

298 During the task, participants were seated comfortably in a cushioned chair with their torso
299 aligned with the edge of a table and their right elbow placed in a padded arm rest. The entire
300 arm was hidden from view with a long occluding board. A 60 cm-long rod (handle length: 12-
301 cm; cross-sectional radius: 0.75 cm) was placed in their right hand. This rod was either
302 wooden (twenty-five participants) or PVC (thirteen participants). The arm was placed at a
303 height necessary for a 1 cm separation between the object (see below) and the rod at a pos-
304 ture parallel with the table. On the surface of the table, an LCD screen (70 x 30 cm) lay
305 backside down in the length-wise orientation; the edge of the LCD screen was 5 cm from the
306 table's edge. The center of the screen was aligned with the participant's midline.

307 The task of participants was to localize touches resulting from active contact between
308 the rod and an object (foam-padded wooden block). In an experimental session, participants
309 completed two tasks with distinct reporting methods (order counterbalanced across partici-
310 pants). In the *image-based task*, participants used a cursor to indicate the corresponding

311 location of touch on a downsized drawing of a rod (20 cm in length; handle to tip); the pur-
312 pose of using a downsized drawing was to dissociate it from the external space occupied by
313 the real rod. The drawing began 15 cm from the edge of the table, was raised 5 cm above
314 the table surface, and was oriented in parallel with the real rod. The red cursor (circle, 0.2
315 cm radius) was constrained to move in the center of the screen occupied by the drawing. In
316 the *space-based task*, participants used a cursor to indicate the corresponding location of
317 touch within an empty LCD screen (white background). The cursor was constrained to move
318 along the vertical bisection of the screen and could be moved across the entire length of the
319 screen. It is critical to note that in this task, participants were forced to rely on somatosenso-
320 ry information about tool length and position as no other sensory cues were available to do
321 so.

322 The trial structure for each task was as follows: In the ‘Pre-contact phase’, partici-
323 pants sat facing the computer screen with their left hand on a trackball. A red cursor was
324 placed at a random location within the vertical bisection of the screen. A ‘go’ cue (brief tap
325 on the right shoulder) indicated that they should actively strike the object with the rod. In the
326 ‘Localization phase’, participants made their task-relevant judgment with the cursor, con-
327 trolled by the trackball. Participants never received feedback about their performance. To
328 minimize auditory cues during the task, pink noise was played continuously over noise-
329 cancelling headphones.

330 The object was placed at one of six locations, ranging from 10 cm from the handle to
331 the tip (10–60 cm from the hand; steps of 10 cm). The number of object locations was un-
332 known to participants. In each task, there were ten trials per touch location, making 60 trials
333 per task and 120 trials in total. The specific location for each trial was chosen pseudo-
334 randomly. The entire experimental session took approximately 45 minutes.

335 The experiment started with a five-minute sensorimotor familiarization session. Par-
336 ticipants were told to explore, at their own pace, how the tool felt to contact the object at dif-
337 ferent locations. They were instructed to pay attention to how the vibrations varied with im-
338 pact location. Visual and auditory feedback of the tool and tool-object contact was prevented

339 with a blindfold and pink noise, respectively. Participants were, however, allowed to hold the
340 object in place with their left hand while contacting it with the tool but were not allowed to
341 haptically explore the rod.

342 At the end of the space-based task, participants used the cursor to report where they
343 felt the tip of the rod (aligned in-parallel to the screen). The judged location of the tip (mean:
344 56.5 cm; SEM: 1.62 cm) was very similar to the rod's actual length (i.e., 60 cm). It is critical
345 to reiterate here that participants had never seen the rod prior up to this point of the experi-
346 ment, and likely relied on somatosensory feedback about its dimensions.

347 **Data Analysis**

348 *Regression analysis*

349 Prior to analysis, all judgments in the image-based task were converted from pixels of draw-
350 ing space to percentage of tool space. All judgments in the space-based task were normal-
351 ized such that their estimated tip location corresponded to 100% of tool space. We then
352 used least-squares linear regression to analyze the localization accuracy. The mean locali-
353 zation judgment for each touch location was modelled as a function of actual object location.
354 Accuracy was assessed by comparing the group-level confidence intervals around the slope
355 and intercept.

356 *Trilateration model*

357 Our model of trilateration in the somatosensory system assumes that the perceived location
358 of touch is a consequence of the optimal integration of two independent location estimates,
359 \tilde{L}_1 and \tilde{L}_2 . This is exemplified in our formulation of trilateration (Equations 1-5). Trilateration
360 predicts that noise in each estimate varies linearly as a function of the distance of touch from
361 two landmarks (Equation 2; Figure 1B), corresponding to the handle and tip. For any location
362 of touch L along a tactile surface, the variance in each landmark-specific location estimate \tilde{L}
363 can therefore be written as follows:

$$\sigma_1^2 = (\hat{\varepsilon}_1 + d_1 \hat{\sigma})^2 \quad (13)$$

$$\sigma_2^2 = (\hat{\varepsilon}_2 + d_2 \hat{\sigma})^2$$

364 in which $\hat{\varepsilon}$ is a landmark-specific intercept term that likely corresponds to uncertainty in the
 365 location of each landmark, d is the distance of touch location L from the landmark (Equa-
 366 tions 2–3), and $\hat{\sigma}$ is the magnitude of noise per unit of distance. We assume that the noise
 367 term $\hat{\sigma}$ corresponds to a general property of the underlying neural network and therefore
 368 model it as the same value for each landmark. The distance-dependent noise for the inte-
 369 grated estimate is therefore:

$$\sigma_{INT} = \sqrt{\frac{\sigma_1^2 \sigma_2^2}{\sigma_1^2 + \sigma_2^2}} \quad (14)$$

370 The three parameters in the model ($\hat{\sigma}$, $\hat{\varepsilon}_1$, and $\hat{\varepsilon}_2$) are properties of the underlying neural
 371 processes that implement trilateration and are therefore not directly observable. They must
 372 therefore be inferred using a reverse engineering approach, where they serve as free pa-
 373 rameters that are fit to each participant's variable errors. We simultaneously fit the three free
 374 parameters to the data using non-linear least squares regression. Optimal parameter values
 375 were obtained through maximum likelihood estimation using the Matlab routine *fmincon*. All
 376 modelling was done with the combined data from both localization tasks. R^2 values for each
 377 participant in each experiment were taken as a measure of the goodness-of-fit between the
 378 observed and predicted pattern of location-dependent noise.

379 *Boundary truncation model*

380 Boundary truncation provides one alternative model to trilateration. This model assumes that
 381 the estimate of location \tilde{L} corresponds to a Gaussian likelihood whose variance is *identical*
 382 at all points on the rod. The inverted U-shaped variability arises because these likelihoods
 383 are truncated by a boundary, either by the range of possible responses or by a categorical
 384 boundary (e.g., between handle and tip). As in Equation 1, we can model each likelihood
 385 $p(\tilde{L}|L)$ as a normal distribution $N(\mu_L, \sigma_L)$ where μ_L is the location of touch L and σ_L is the

386 standard deviation. The posterior estimate $p(L|\tilde{L})$ then corresponds to a likelihood truncated
387 at γ_1 and γ_2 , where $\gamma_2 > \gamma_1$. Doing so will distort the mean and variance of the posterior es-
388 timate.

389 We fit this truncation model to the participant-level variable errors in each of our ex-
390 periments. The standard deviation for each location, $\sigma_T(L)$, was determined by truncating a
391 normal distribution at γ_1 and γ_2 using the *makedist* and *truncate* functions in MATLAB. The
392 model therefore had three free parameters, σ_T , γ_1 and γ_2 . The value of σ_T was constrained
393 between 1 and 40; γ_1 between -30 and 30; and γ_2 between 70 and 130 (units: % of rod sur-
394 face). These ranges—particularly for γ_1 and γ_2 —are quite unrealistic but were chosen to
395 maximize a good fit with the variable errors. Fitting procedures for this model were the same
396 as the trilateration model.

397 *Model comparisons*

398 We used the Bayesian Information Criterion (BIC) to compare the boundary and trilateration
399 models. The difference in the BIC (ΔBIC) was used to determine a significant difference in
400 fit. Consistent with convention, the chosen cutoff for moderate evidence was a ΔBIC of 2 and
401 the cutoff for strong evidence was a ΔBIC of 6.

402 **Results**

403 *Accurate localization of touch on a tool*

404 In the current experiment ($n=38$), we investigated whether tactile localization on a 60-cm
 405 hand-held rod is characterized by the U-shaped pattern of variability (Figure 1B) that is
 406 characteristic of trilateration when localizing touch on the body. In two tasks, we measured

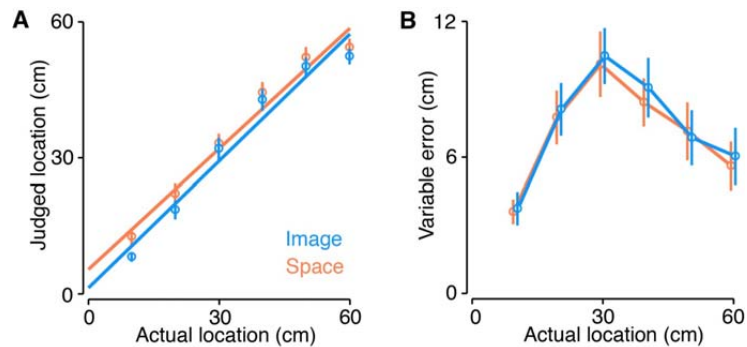


Figure 4. Localization and variable error for both tasks

(A) Regressions fit to the localization judgments for both the image-based (blue) and space-based (orange) tasks. Error bars correspond to the group-level 95% confidence interval. (B) Group-level variable errors for both tasks. Error bars correspond to the group-level 95% confidence interval.

407 participants' ability to localize an object that was actively contacted with a hand-held tool. In
 408 the *image-based task*, participants indicated the point of touch on a downsized drawing of
 409 the tool. In the *space-based task*, participants indicated the point of touch in external space.
 410 The latter task ensured that localization was not truncated by boundaries in the range of
 411 possible responses.

412 Consistent with prior results (Miller et al., 2018), we found that participants were
 413 generally quite accurate at localizing touch on the tool. Linear regressions (Figure 4A) com-
 414 paring perceived and actual hit location found slopes near unity both the image-based task
 415 (mean slope: 0.93, 95% CI [0.88, 0.99]) and the space-based task (mean slope: 0.89, 95%
 416 CI [0.82, 0.95]). Analysis of the variable errors (2x6 repeated measures ANOVA) found a
 417 significant main effect of hit location ($F(5,185)=36.1$, $p<.001$) but no main effect of task
 418 ($F(1,37)=0.39$, $p=.54$) or an interaction ($F(5,185)=0.21$, $p=.96$). Crucially, the pattern of vari-

419 able errors (Figure 4B) in both tasks displayed the hypothesized inverted U-shape, which
 420 was of similar magnitude to what has been observed for touch on the arm (Cholewiak and
 421 Collins, 2003; Miller et al., 2022).

422 *Computational modelling of behavior*

423 We next used computational modelling to confirm that the observed pattern of variable er-
 424 rors was indeed due to trilateration. We fit each participant's variable errors with a probabilis-
 425 tic model of optimal trilateration (Figure 1A-B) that was derived from its theoretical formula-
 426 tion (see Methods). We compared the trilateration model to an alternative hypothesis: The
 427 inverted U-shaped pattern is due to truncation at the boundaries of localization (Petzschner
 428 et al., 2015), which cuts off the range of possible responses and thus produces lower varia-
 429 bility at these boundaries. We fit a boundary truncation model to directly compare to our tri-
 430 lateration model. Given the lack of a main effect of task and to increase statistical power, we
 431 collapsed across both tasks in this analysis.

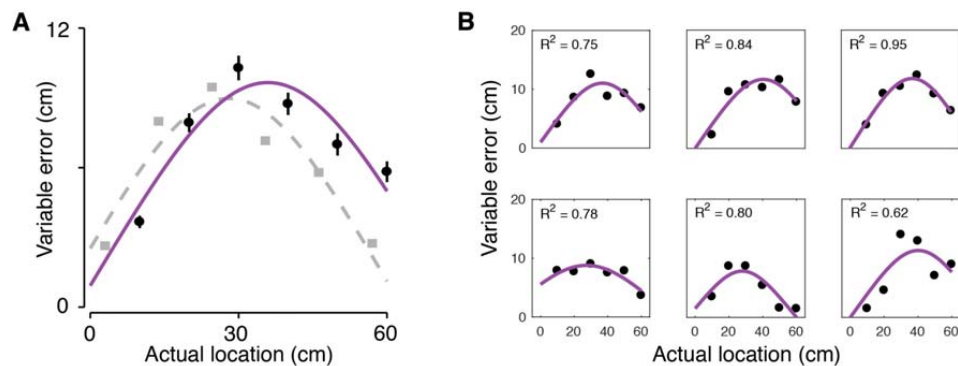


Figure 5. Trilateration model provides a good fit to localization behavior

(A) Fit of the trilateration model to the group-level variable error (black dots). The purple line corresponds to the model fit. The light gray line and squares correspond to variable errors for localization on the arm observed in Miller et al (2022); note that this data is size adjusted to account for differences in arm and rod size. (B) Fit of the trilateration model to the variable errors of six randomly chosen participants. The fit of the trilateration model for each participant's behavior can be seen in Extended Data Figure 5-1 and 5-2.

432 Our computational model of trilateration provided a good fit to the variable errors ob-
 433 served during tactile localization on a tool. This was evident at the group-level, where the
 434 magnitude of variable errors was similar to what has been found when localizing touch on
 435 the arm (Figure 5A). We further observed a high coefficient of determination at the level of
 436 individual participants (median R^2 : 0.75; range: 0.29–0.95); indeed, 30 out of 38 participants
 437 had an $R^2 > 0.6$. The fits of the trilateration model to the data of 6 randomly chosen partici-
 438 pants can be seen in Figure 5B. The fits of the trilateration model each participant's behavior

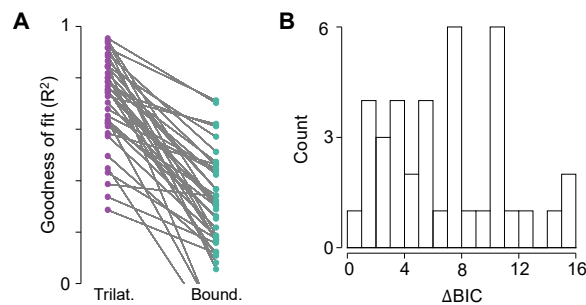


Figure 6. Trilateration provides a better fit to the data than boundary truncation

(A) Participant-level goodness of fits (R^2) for the trilateration model (left, purple) and the boundary truncation model (right, green). For each participant, trilateration was a better fit to the data. (B) Histogram of the ΔBIC values used to adjudicate between the two models, color-coded by the strength of the evidence in favor of trilateration. Purple corresponds to substantial evidence in favor of trilateration; pink corresponds to moderate evidence in favor of trilateration; gray corresponds to weak/equivocal evidence in favor of trilateration. Note that in no case did the boundary truncation model provide a better fit to the localization data (i.e., $\Delta BIC < 0$).

439 can be seen in Extended Data Figures 5-1 and 5-2. In contrast, the R^2 of the boundary trun-
 440 cation model was substantially lower than the trilateration model (median: 0.30; range: -
 441 0.19–0.71), never showing a better fit to the data in any participant (Figure 6A).

442 We next compared each model directly using the Bayesian Information Criteria (BIC).
 443 The BIC score for the trilateration model was lower in all 38 participants (mean \pm sd; Trilatera-
 444 tion: 11.88 ± 5.88 ; Truncation: 18.74 ± 4.70). Statistically, 33 participants showed moderate

445 evidence ($\Delta\text{BIC}>2$) and 20 participants showed strong evidence ($\Delta\text{BIC}>6$) in favor of trilateration (Figure 6B). In total, our results strongly suggest that, as with the body, localizing touch on a tool is consistent with a computation via trilateration.

448 *Neural network simulations*

449 Finally, we simulated trilateration on a tool using a biologically inspired neural network with a similar architecture as we have done previously. The goal of these simulations was to concretely demonstrate that the feature space of vibratory motifs could stand in for the physical space of the rod. Our neural network thus took the mode amplitudes as input and trilaterated the resulting touch location in tool-centered coordinates (5000 simulations per location).

454 Both the mode and feature space layers of the neural network (Figure 3, bottom and middle) produced unbiased sensory estimates with minimal uncertainty (Extended Data Figure 7-1). Crucially, both subpopulations in the distance-computing layer (Layer 3; Figure 3, top) were able to localize touch with minimal constant error (Figure 7A, upper panel), demonstrating that each could produce unbiased estimates of location from the sensory input. However, as predicted given the gradient in tuning parameters, the noise in their estimates rapidly increased as a function of distance from each landmark (Figure 7B upper panel), forming an X-shaped pattern across the surface of the tool.

462 We next examined the output of the Bayesian decoder from Equations 11–12 (Fig-
 463 ure 7, lower panel). As expected, we observed the computational signature of trilateration.
 464 Integrating both estimates resulted in an inverted U-shaped pattern of decoding noise across

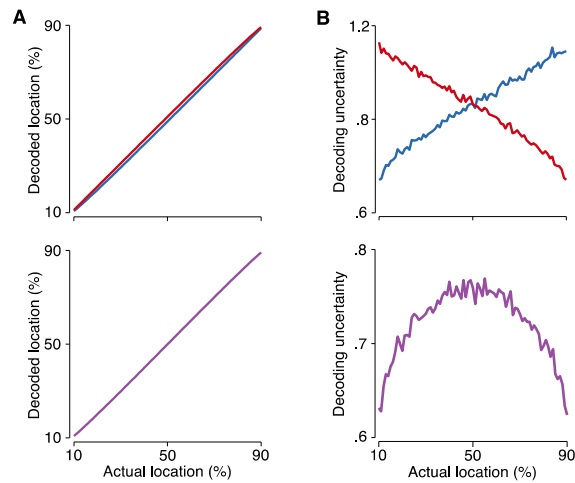


Figure 7. Neural network simulations

(A) Localization accuracy for the estimates of each decoding subpopulation (upper panel; L₁, blue; L₂, red) and after integration by the Bayesian decoder (lower panel; L_{INT}, purple). (B) Decoding noise for each decoding subpopulation (upper panel) increased as a function of distance from each landmark. Note that distance estimates are made from the 10% and 90% locations for the first (blue) and second (red) decoding subpopulations, respectively. Integration via the Bayesian decoder (lower panel) led to an inverted U-shaped pattern across the surface. Note the differences in the y-axis range for both panels. The results of decoding for the mode and feature space layers of the network can be seen in Extended Data Figure 7-1.

465 the surface of the tool (Figure 7B, lower panel), with the lowest decoding noise near the
 466 landmarks and the highest decoding variance in the middle. Crucially, this is the exact pat-
 467 tern of variability we observed in our behavioral experiments (see above) and have previous-
 468 ly observed for tactile localization on the body. These simulations establish the plausibility of
 469 trilateration as a computation that can turn a vibratory code into a spatial representation.

470 **Discussion**

471 If tools are embodied by the sensorimotor system, we would expect that the brain repurpos-
472 es its body-based sensorimotor computations to perform similar tasks with tools. Using tac-
473 tile localization as our case study, we uncovered multiple pieces of evidence that are con-
474 sistent with this embodied view. First, as is the case for body parts, we observed that localiz-
475 ing touch on the surface of a tool is characterized by perceptual anchors at the handle and
476 tip (de Vignemont et al., 2009). Second, computational modeling of behavioral responses
477 suggests that they are the result of the probabilistic computation involving trilateration. In-
478 deed, perceptual anchors are a computational signature of trilateration. Finally, using a sim-
479 ple three-layer population-based neural network, we demonstrated the possibility of trilatera-
480 tion in the vibratory feature space evoked by touches on tools. This neural network trans-
481 formed a vibration-based input into a spatial code, reproducing perceptual anchors on the
482 tool surface. These findings go well-beyond prior research on embodiment (Martel et al.,
483 2016) by identifying a computation that functionally unifies tools and limbs. Indeed, they
484 suggest that trilateration is a spatial computation employed by the somatosensory system to
485 localize touch on body parts and tools alike (Miller et al., 2022). They further have important
486 implications for how trilateration would be repurposed at a neural level for tool-extended
487 sensing.

488 If trilateration is a fundamental spatial computation used by the somatosensory sys-
489 tem, it should be employed to solve the same problem (i.e., localization) regardless of
490 whether the sensory surface is the body or a tool. Previous tactile localization studies have
491 reported increased perceptual precision near the boundaries of the hands (Elithorn et al.,
492 1953; Miller et al., 2022), arm (Cholewiak and Collins, 2003; de Vignemont et al., 2009;
493 Miller et al., 2022), feet (Halnan and Wright, 1960), and abdomen (Cholewiak et al., 2004).
494 These perceptual anchors are a signature of a trilateration computation (Miller et al., 2022).
495 The results of the present study are consistent with the use of trilateration to localize touch
496 on tools as well.

497 Our findings provide computational evidence that tools are *embodied* in the sen-
498 sorimotor system (Martel et al., 2016), an idea that was proposed over a century ago (Head

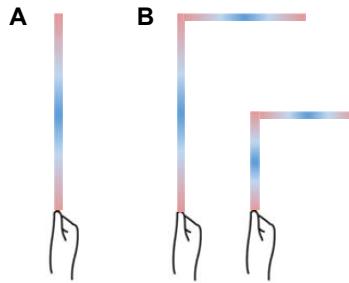


Figure 8. Simulations of multisegmented rods

We simulated how trilateration operates within rods with different numbers of segments. Here we show the predicted patterns of variability for (A) a single-segment rod (used in present study) and, (B) two-segment (left) and three-segment (right) rods. The magnitude of variable error is color-coded as red-to-blue (low-to-high). The inverted U-shaped pattern of variability was observed in each segment.

499 and Holmes, 1911). The close functional link between tools and limbs is not just a superficial
500 resemblance but rather a reflection of the repurposing of neurocomputational resources ded-
501 icated to sensing and acting with a limb to that with a tool (Makin et al., 2017). This repur-
502 posing may be one reason that tool use leads to measurable changes in body perception
503 and action processes (Canzoneri et al., 2013; Cardinali et al., 2009; Miller et al., 2014; Miller
504 et al., 2019a).

505 Whereas the present study focused on simply-shaped tools (i.e., straight rods), tac-
506 tile localization is also possible on more complexly-shaped tools (Yamamoto et al., 2005).
507 We propose that trilateration also underlies tactile localization on these tools. We leveraged
508 our trilateration model to simulate patterns of tactile localization on rods with different num-
509 bers of segments (Figure 8). For multisegmented limbs (e.g., the arm), trilateration occurs
510 locally within each segment (Cholewiak and Collins, 2003; Miller et al., 2022). That is, the
511 signature inverted U-shaped pattern of variability is observed within each segment (e.g., up-
512 per and lower arms). Our simulations suggested that the same would be true for mul-

513 tisegmented tools (Figure 8B). We predict that tactile localization within each segment of a
514 rod would be characterized by the signature pattern of variability indicative of trilateration.

515 Even though trilateration was repurposed for localizing touch on a rod, we observed
516 a noticeable difference in the overall shape of variable error between localizing touch on a
517 rod versus limb (e.g., the arm; Figure 5A). Whereas localization uncertainty (i.e., variable
518 error) is typically symmetric about the center of a limb (Miller et al., 2022), uncertainty was
519 asymmetric for the rod. Specifically, variable errors were lower near the handle than the tip,
520 peaking away from the center of the rod and towards the tip. These patterns of variable error
521 were also visible in the behavior of individual participants (Extended Data Figures 5-1 and 5-
522 2) and are a direct consequence of differences in the baseline uncertainty of each distance
523 estimate (Equation 13), as demonstrated by simulations in Miller et al., (2022).

524 There are at least two potential sources for these differences in baseline uncertainty.
525 First, striking the rod near the tip may produce less consistent sensory information (i.e., vi-
526 brations), translating into greater sensory uncertainty of where the rod is touched. However,
527 this explanation is unlikely since the hypothesized differences in sensory consistency were
528 not observed in a previous study that characterized a rod's vibratory motifs (Miller et al.,
529 2018). Instead, the source of this difference may lie in the uncertainty of where each bound-
530 ary is perceived in space via proprioceptive feedback (Equation 3). The location of the han-
531 dle is well-defined, as it corresponds to the position of the hand. The location of the tip is
532 less well-defined, as it must be extracted indirectly from proprioceptive feedback from the
533 forelimb (Debats et al., 2012). This likely corresponds to higher estimation uncertainty of its
534 position in space, contributing to greater baseline uncertainty of the tip-based distance esti-
535 mate (Equation 13). Future studies should attempt to adjudicate between these two hypoth-
536 eses.

537 Another important difference between limbs and tools is the sensory input used to
538 derive localization estimates. While the skin is innervated with sensory receptors, the soma-
539 tosensory system must 'tune into' a tool's mechanical response to extract meaningful infor-
540 mation from it. It was previously proposed that where a rod is touched is encoded by the

541 amplitudes of its resonant responses when contacting an object (Miller et al., 2018; Miller et
542 al., 2019b). These resonant modes form a feature space that is isomorphic with the physical
543 space of the tool. At a peripheral level, these resonances are re-encoded by the spiking pat-
544 terns of tactile mechanoreceptors (Johnson, 2001). Therefore, unlike for touch on the body,
545 localizing touch on a tool requires the somatosensory system to perform a temporal-to-
546 spatial transformation.

547 We used neural network simulations to embody the necessary transformations to im-
548 plement trilateration on a tool. Our neural network assumes that the human brain contains
549 neural populations that encode for the full feature space of rod vibration. While very little is
550 known about how these types of naturalistic vibrations are represented by the somatosenso-
551 ry system, our modeling results and prior research (Miller et al., 2018; Miller et al., 2019)
552 suggest that there are neural populations that encode their properties. Previous work
553 demonstrated that individual neurons in primary somatosensory cortex multiplex both ampli-
554 tude and frequency in their firing properties (Harvey et al., 2013). Recent evidence further
555 suggests that human S1 is tuned to individual vibration frequencies (Wang and Yau, 2021).
556 Our neural network modelling assumes that there are also neurons tuned to the amplitude of
557 specific frequencies, though direct empirical evidence for this tuning is currently lacking. The
558 existence of this coding would be consistent with the finding that S1 performs the initial
559 stages of localization on a rod (Miller et al., 2019). Furthermore, resonant amplitudes are
560 crucial pieces of information in the natural statistics of vibrations, making it plausible that
561 they are encoded at some stage of processing. Our results therefore open up a new avenue
562 for neurophysiological investigations into how naturalistic vibrations are encoded by the so-
563 matosensory system.

564 The present study demonstrates the biological possibility that the resonant feature
565 space can stand in for the physical space of the tool, allowing for trilateration to be per-
566 formed to localize touch in tool-centered coordinates. It is interesting to note that the present
567 neural network had a similar structure to one we previously demonstrated could perform tri-
568 lateration on the body surface. The biggest difference is the input layer, which must first en-

569 code the vibration information. However, once this is transformed into the representation of
570 the feature space, the computation proceeds as it would for the body. Note that this does not
571 necessitate that the same neural populations localize touch on limbs and tools (Schone et
572 al., 2021), but only that the same computation is performed when localizing touch on both
573 surfaces. Our network therefore provides a concrete demonstration of what it means to re-
574 purpose a body-based computation to localize touch on a tool. The repurposing of the neural
575 network architecture for trilateration explains tool embodiment and the emergence of a
576 shared spatial code between tools and skin.

577 **Data and code availability**

578 All data and code will be available in a repository upon acceptance of the manuscript.

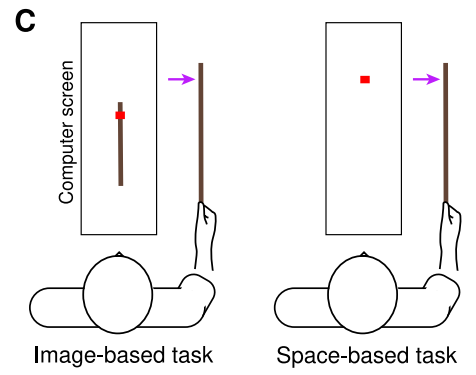
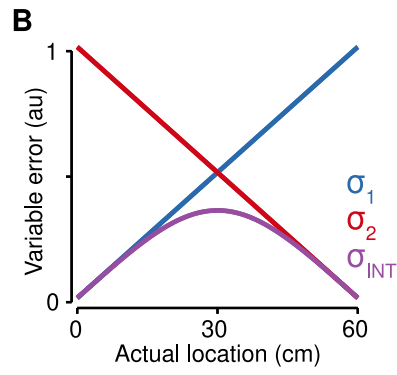
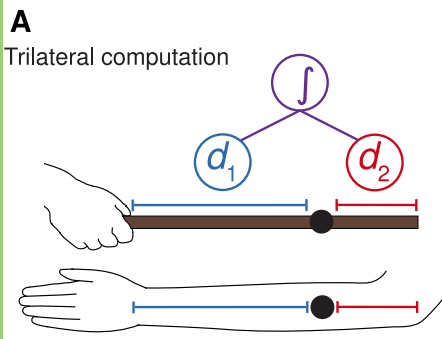
579

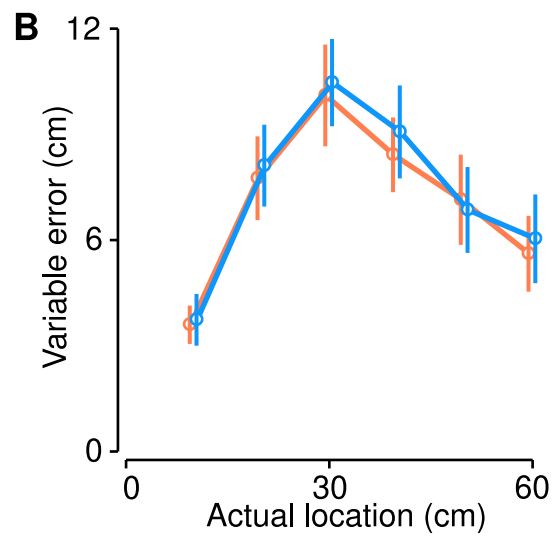
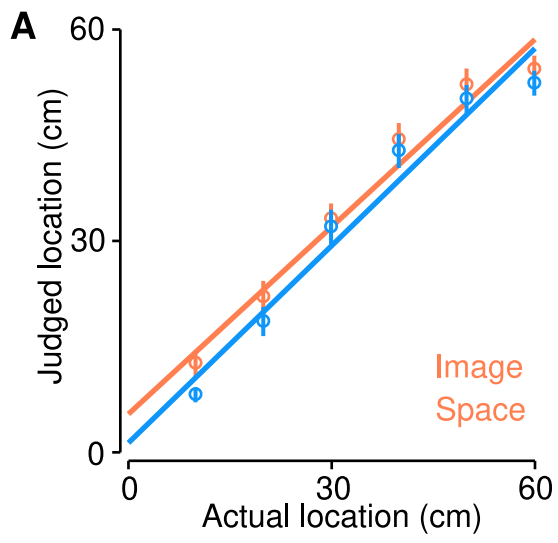
580 **References**

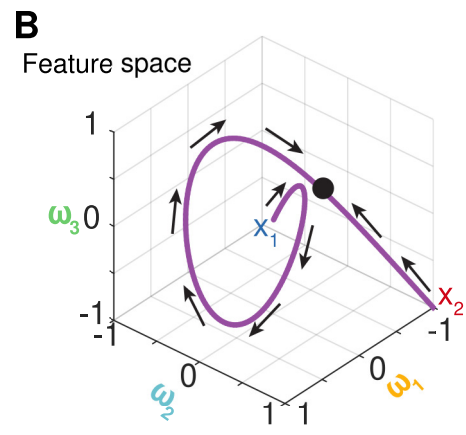
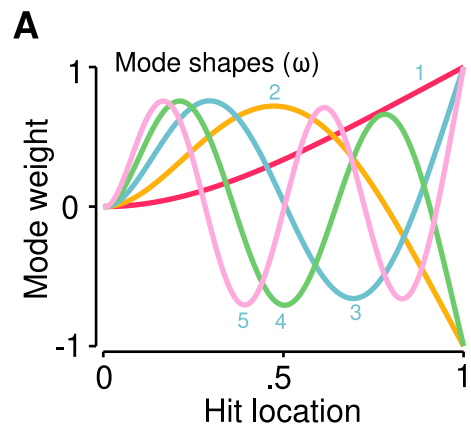
- 581 Canzoneri E, Ubaldi S, Rastelli V, Finisguerra A, Bassolino M, Serino A (2013) Tool-use
582 reshapes the boundaries of body and peripersonal space representations.
583 *Experimental brain research* 228:25-42.
- 584 Cardinali L, Brozzoli C, Finos L, Roy A, Farnè A (2016) The rules of tool incorporation: Tool
585 morpho-functional & sensori-motor constraints. *Cognition* 149:1-5.
- 586 Cardinali L, Frassinetti F, Brozzoli C, Urquizar C, Roy AC, Farnè A (2009) Tool-use induces
587 morphological updating of the body schema. *Current Biology* 19:R478-479.
- 588 Cardinali L, Brozzoli C, Urquizar C, Salemme R, Roy A, Farnè A (2011) When action is not
589 enough: tool-use reveals tactile-dependent access to body schema.
590 *Neuropsychologia* 49:3750-3757.
- 591 Cardinali L, Jacobs S, Brozzoli C, Frassinetti F, Roy AC, Farnè A (2012) Grab an object with
592 a tool and change your body: tool-use-dependent changes of body representation for
593 action. *Experimental Brain Research* 218:259-271.
- 594 Cholewiak RW, Collins AA (2003) Vibrotactile localization on the arm: Effects of place,
595 space, and age. *Percept Psychophys* 65:1058-1077.
- 596 Cholewiak RW, Brill JC, Schwab A (2004) Vibrotactile localization on the abdomen: effects
597 of place and space. *Percept Psychophys* 66:970-987.
- 598 Clemens IA, De Vrijer M, Selen LP, Van Gisbergen JA, Medendorp WP (2011) Multisensory
599 processing in spatial orientation: an inverse probabilistic approach. *J Neurosci*
600 31:5365-5377.
- 601 de Vignemont F, Majid A, Jola C, Haggard P (2009) Segmenting the body into parts:
602 evidence from biases in tactile perception. *Q J Exp Psychol (Hove)* 62:500-512.
- 603 Debats NB, Kingma I, Beek PJ, Smeets JB (2012) Moving the weber fraction: the perceptual
604 precision for moment of inertia increases with exploration force. *PLoS One* 7:e42941.
- 605 Delhaye BP, Long KH, Bensmaia SJ (2018) Neural Basis of Touch and Proprioception in
606 Primate Cortex. *Compr Physiol* 8:1575-1602.
- 607 Elithorn A, Piercy MF, Crosskey MA (1953) Tactile Localization. *Quarterly Journal of*
608 *Experimental Psychology* 5:171-182.
- 609 Ernst MO, Banks MS (2002) Humans integrate visual and haptic information in a statistically
610 optimal fashion. *Nature*.
- 611 Fabio C, Salemme R, Farnè A, Miller LE (2021) Alpha oscillations are involved in localizing
612 touch on a tool. *Journal of cognitive neuroscience* 34:675-686
- 613 Faisal AA, Selen LP, Wolpert DM (2008) Noise in the nervous system. *Nat Rev Neurosci*
614 9:292-303.
- 615 Garbarini F, Fossataro C, Berti A, Gindri P, Romano D, Pia L, della Gatta F, Maravita A,
616 Neppi-Modona M (2015) When your arm becomes mine: pathological embodiment of
617 alien limbs using tools modulates own body representation. *Neuropsychologia*
618 70:402-413.

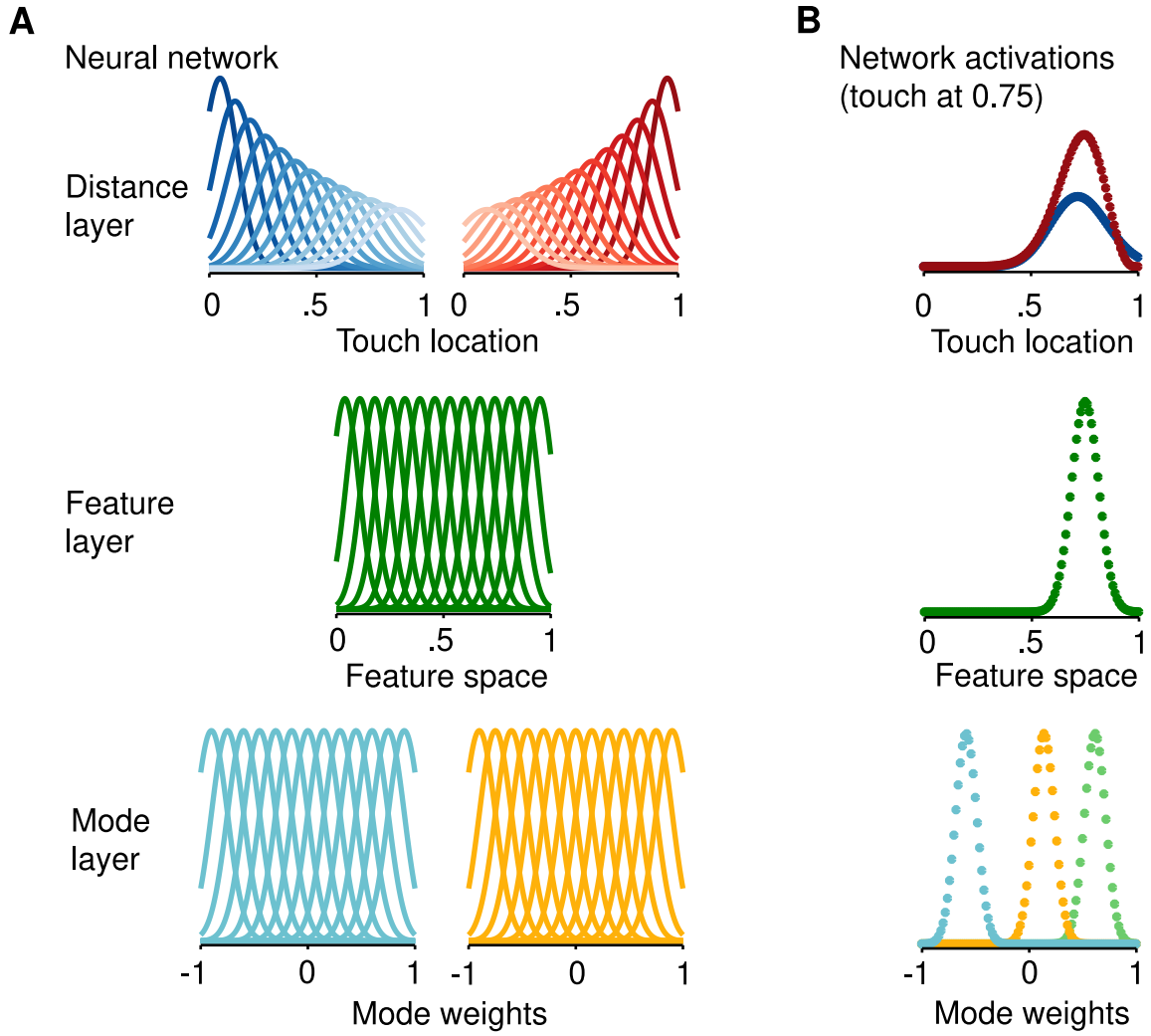
- 619 Halnan CR, Wright GH (1960) Tactile Localization. *Brain* 83:677-700.
- 620 Harvey MA, Saal HP, Dammann JF, 3rd, Bensmaia SJ (2013) Multiplexing stimulus
621 information through rate and temporal codes in primate somatosensory cortex. *PLoS*
622 *Biol* 11:e1001558.
- 623 Head H, Holmes G (1911) Sensory disturbances from cerebral lesions. *Brain* 34:102-254.
- 624 Imamizu H, Miyauchi S, Tamada T, Sasaki Y, Takino R, PuÉtz B, Yoshioka T, Kawato M
625 (2000) Human cerebellar activity reflecting an acquired internal model of a new tool.
626 *Nature* 403:192-195.
- 627 Jazayeri M, Movshon JA (2006) Optimal representation of sensory information by neural
628 populations. *Nat Neurosci* 9:690-696.
- 629 Johansson RS, Flanagan JR (2009) Coding and use of tactile signals from the fingertips in
630 object manipulation tasks. *Nat Rev Neurosci* 10:345-359.
- 631 Kilteni K, Ehrsson HH (2017) Sensorimotor predictions and tool use: Hand-held tools
632 attenuate self-touch. *Cognition* 165:1-9.
- 633 Kording KP, Wolpert DM (2004) Bayesian integration in sensorimotor learning. *Nature*
634 427:244-247.
- 635 Longo MR, Azanon E, Haggard P (2010) More than skin deep: body representation beyond
636 primary somatosensory cortex. *Neuropsychologia* 48:655-668.
- 637 Ma WJ, Beck JM, Latham PE, Pouget A (2006) Bayesian inference with probabilistic
638 population codes. *Nat Neurosci* 9:1432-1438.
- 639 Makin TR, de Vignemont F, Faisal AA (2017) Neurocognitive barriers to the embodiment of
640 technology. *Nature Biomedical Engineering* 1.
- 641 Maravita A, Iriki A (2004) Tools for the body (schema). *Trends Cogn Sci* 8:79-86.
- 642 Martel M, Cardinali L, Roy AC, Farne A (2016) Tool-use: An open window into body
643 representation and its plasticity. *Cognitive Neuropsychology* 33:82-101.
- 644 Martel M, Cardinali L, Bertonati G, Jouffrais C, Finos L, Farnè A, Roy AC (2019)
645 Somatosensory-guided tool use modifies arm representation for action. *Scientific*
646 *reports* 9:1-14.
- 647 Medina J, Coslett HB (2010) From maps to form to space: touch and the body schema.
648 *Neuropsychologia* 48:645-654.
- 649 Miller LE, Longo MR, Saygin AP (2014) Tool morphology constrains the effects of tool use
650 on body representations. *J Exp Psychol Hum Percept Perform* 40:2143-2153.
- 651 Miller LE, Longo MR, Saygin AP (2017) Visual illusion of tool use recalibrates tactile
652 perception. *Cognition* 162:32-40.
- 653 Miller LE, Longo MR, Saygin AP (2019b) Tool use modulates somatosensory cortical
654 processing in humans. *Journal of cognitive neuroscience* 31:1782-1795.
- 655 Miller LE, Montroni L, Koun E, Salemme R, Hayward V, Farne A (2018) Sensing with tools
656 extends somatosensory processing beyond the body. *Nature* 561:239-242.

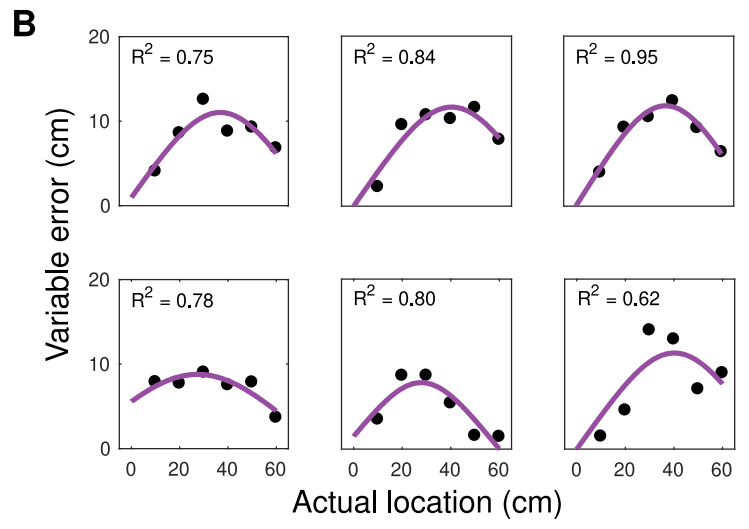
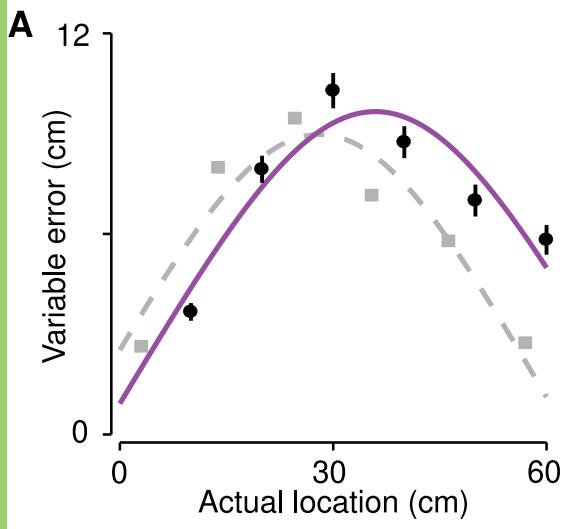
- 657 Miller LE, Fabio C, Azoural M, Muret D, van Beers R, Farnè A, Medendorp WP (2022) A
658 neural surveyor to map touch on the body. *Proceedings of the National Academy of*
659 *Sciences* 119.
- 660 Miller LE, Fabio C, Ravenda V, Bahmad S, Koun E, Salemm R, Luaute J, Bolognini N,
661 Hayward V, Farnè A (2019) Somatosensory Cortex Efficiently Processes Touch
662 Located Beyond the Body. *Curr Biol* 29:4276-4283 e4275.
- 663 Nieder A, Miller EK (2003) Coding of cognitive magnitude: compressed scaling of numerical
664 information in the primate prefrontal cortex. *Neuron* 37:149-157.
- 665 Pazen M, Uhlmann L, van Kemenade BM, Steinsträter O, Straube B, Kircher T (2020)
666 Predictive perception of self-generated movements: commonalities and differences in
667 the neural processing of tool and hand actions. *NeuroImage* 206:116309.
- 668 Petzschner FH, Glasauer S, Stephan KE (2015) A Bayesian perspective on magnitude
669 estimation. *Trends Cogn Sci* 19:285-293.
- 670 Pouget A, Beck JM, Ma WJ, Latham PE (2013) Probabilistic brains: knowns and unknowns.
671 *Nat Neurosci* 16:1170-1178.
- 672 Romano D, Uberti E, Caggiano P, Cocchini G, Maravita A (2019) Different tool training
673 induces specific effects on body metric representation. *Experimental brain research*
674 237:493-501.
- 675 Schone HR, Mor ROM, Baker CI, Makin TR (2021) Expert tool users show increased
676 differentiation between visual representations of hands and tools. *Journal of*
677 *Neuroscience*.
- 678 Sposito A, Bolognini N, Vallar G, Maravita A (2012) Extension of perceived arm length
679 following tool-use: clues to plasticity of body metrics. *Neuropsychologia* 50:2187-
680 2194.
- 681 Wang L, Yau JM (2021) Signatures of vibration frequency tuning in human neocortex.
682 *bioRxiv*.
- 683 Yamamoto S, Kitazawa S (2001) Sensation at the tips of invisible tools. *Nature neuroscience*
684 4:979-980.
- 685 Yamamoto S, Moizumi S, Kitazawa S (2005) Referral of tactile sensation to the tips of L-
686 shaped sticks. *Journal of Neurophysiology* 93:2856-2863.
687

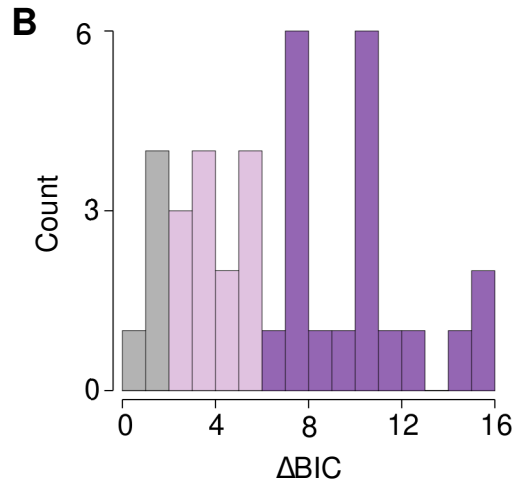
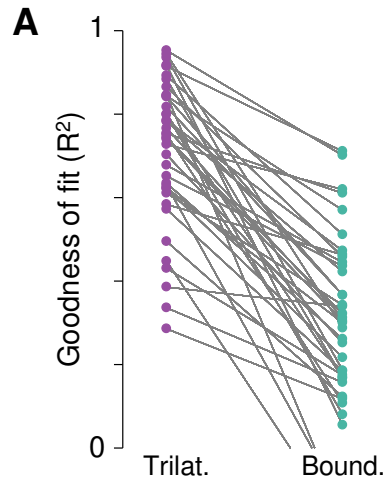


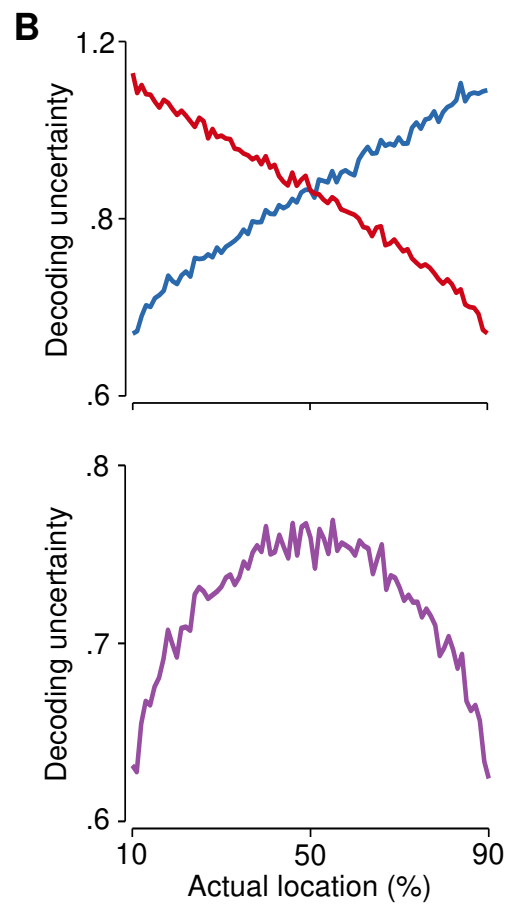
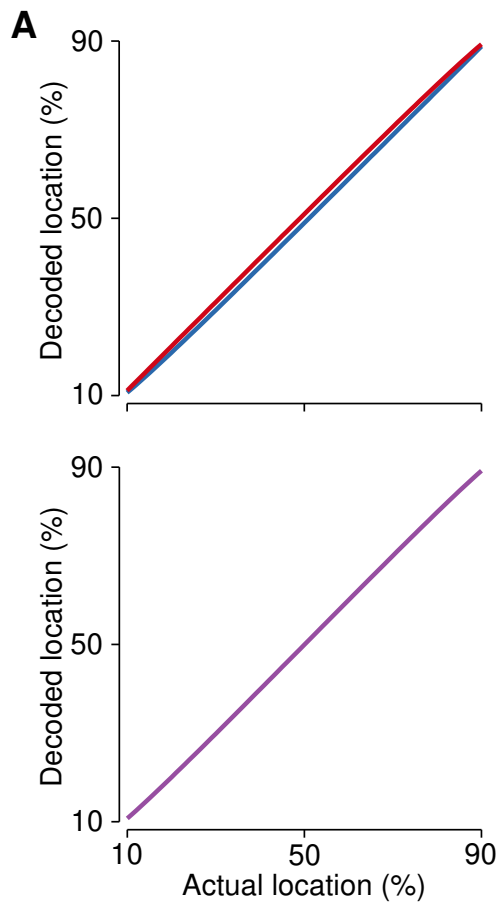












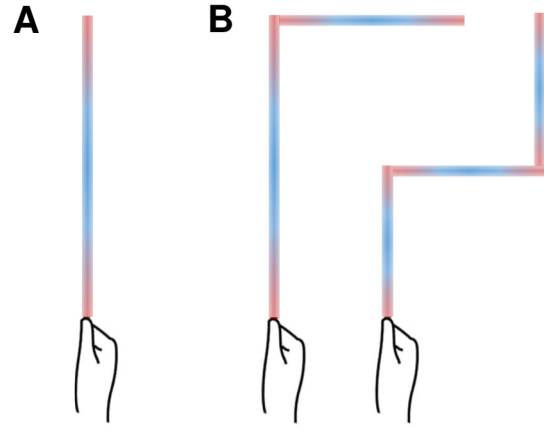


Table 1. Neural network parameter values

	$\sqrt{f^M}$	$\sqrt{f^S}$	$\sqrt{f^{D1}}$	$\sqrt{f^{D2}}$
μ	-1.5:0.02:1.5	-40:1:140	0:1:140	-40:1:100
κ or κ_0	25	25	25	25
σ or σ_0	0.08	3.40	3.40	3.40
β	—	—	0.01	0.01
ν	—	—	0.5	0.5